IEEE Access
Multidisciplinary | Rapid Review | Open Access Journal

Received 10 July 2023, accepted 28 July 2023, date of publication 7 August 2023, date of current version 14 August 2023.

Digital Object Identifier 10.1109/ACCESS.2023.3303333

RESEARCH ARTICLE

Efficient Ultra Wideband Radar Based Non Invasive Early Breast Cancer Detection

M. K. DEVIKA MENON AND JOSEPH RODRIGUES
Department of Electrical and Electronics Engineering, CHRIST (Deemed to be University), Bengaluru 560074, India
Corresponding author: M. K. Devika Menon (devika.menon@christuniversity.in)

This work was supported in part by the Centre of Research, CHRIST (Deemed to be University), Bengaluru under Seed Money Grant received for the Project titled "Design of Ultra Wideband Wireless Body Area Network for Non Invasive Tumor Detection."

ABSTRACT Ultra Wideband radar systems have emerged as a good alternative for non-invasive and harmless breast cancer detection. In this paper, bistatic and monostatic radar systems are proposed, which detects the deep-rooted and smallest formation of the tumor in the breast. The source signal for transmission through the breast is a seventh derivative Gaussian Ultra Wideband pulse. This pulse is shaped using the proposed sharp transition bandpass Finite Impulse Response filter. The pulse shaper filter design has a sharp transition, hence efficient for shaping very short-duration pulses, achieving higher data rate and less interference issues. Also, the pulse tightly fits the Federal Communication Commission spectral mask, thus achieving higher spectral utilization efficiency and meeting the signal safety standards for transmission through the breast. The shaped pulse fed to the antenna of the radar system provides higher antenna radiation efficiency and radiating power due to the concentration of power in the main lobe, sidelobe suppression, and less channel loss. Tumor detection is based on the time and frequency domain analysis of the backscattered signals from the tumor. These signals have higher amplitude, higher electric field intensity variations, and an increase in the scattering parameter values due to the presence of tumor. Simulation results show significant changes in the electric field intensity for normal and malignant breast tissue for tumor sizes ranging from 4 mm to 0.5 mm. To accurately detect the location of tumor inside the breast, Specific Absorption Rate (SAR) analysis is carried out. It is observed that the energy absorption in the cancerous breast is higher than that of the normal breast, thereby aids to detect the location of the tumor accurately by identifying the coordinates of the maximum value of SAR. The results obtained with an experimental setup consisting of fabricated heterogeneous breast phantom with tumor and monostatic radar closely confirms with the simulation results.

INDEX TERMS Breast phantom, early breast cancer detection, Cole-Cole model, dielectric properties, federal communication commission mask, scattering parameter, specific absorption rate, ultra wideband pulse shaper, ultra wideband radar.

I. INTRODUCTION

Ultra-wideband (UWB) is a viable option for short range radio communication required for human non-invasive ailment detection, prevention, and in wireless body area networks [1]. UWB signals have no ionizing impacts and have better penetration capability to different materials making it a good choice for several applications related to human ailments [2], [3]. UWB technology is used to image surface and deeper structures like breast tissues. UWB radio pulse transmission has reduced electromagnetic interference issues [4]. UWB pulses employed for antenna wave propagation inside the body are mainly Gaussian, Hermitian, and Discrete Prolate Spheroidal [5]. Basic Gaussian is not versatile for effective use of the spectrum and flexible interference mitigation [6]. So, derivative pulses of higher order are employed. Hence the pulse roll-off gets better with the center frequency shifted to higher frequencies and the low power spectrum distributed to lower frequencies. To fit the Federal Communication Commission (FCC) mask, the

The associate editor coordinating the review of this manuscript and approving it for publication was Dušan Grujić.

order of derivative pulse is increased, which in turn increases the hardware required [7]. The seventh derivative Gaussian pulse is a suitable pulse for Impulse Radio Ultra Wideband (IR-UWB) indoor applications, with its spectrum complying with FCC mask for indoor systems applications. The signal transmission in Impulse Radio (IR) transmission systems has a simple setup, reduced power consumption, and can be miniaturized [8], [9]. The drawback of UWB signal while propagating through the human body, classified as IEEE 802.15.6, is the high attenuation of Radio Frequency (RF) wave inside the body due to its high frequency involved and the dielectric nature of the body [1]. The received pulses are distorted due to the loss characteristics of body composition, which are frequency dependent and reflection of waves from various tissues [10]. Reduction in attenuation is therefore very important to increase the signal strength of the UWB signal while propagating through breast tissue, which makes up the propagation channel, and thereby detect tumor of small size at a very early stage [11].

The transmit power spectrum in UWB systems is limited by spectral mask specifications. Hence, pulse shape design for UWB pulse is necessary to achieve optimal spectrum utilization, spectral mask compatibility, and coexistence with other wireless systems. In the UWB radar detection approach, short duration IR shaped UWB pulses by employing bandpass Finite Impulse Response (FIR) filters are transmitted into the body using a suitable transmitting antenna [11]. These shaped pulses have better Spectral Utilization Efficiency (SUE), less ringing effect, improved Bit Error Rate (BER), lower Side Lobe Level (SLL), reduced clutter, image resolution improvement, eliminate undesired frequency components, and satisfies the FCC mask [12].

Pulse shaping using filters can be implemented using digital linear phase FIR filters to improve power in the main lobe by employing sharp transition filters dealt in literature [13], [14], [15]. A sharp transition filter with desired passband and stopband specifications and acceptable magnitude response is difficult to design and requires large filter order. Conventional methods for sharp transition FIR filters using window functions and frequency sampling methods require high filter order. The numeric Remez approach, which employs optimization techniques, requires lower filter order, but computational complexity is high. They do not yield an explicit expression for the filter transfer function. Hence it is difficult to tune to the desired magnitude responses like application dealt in this paper. Synthesis of sharp transition FIR filters using simple analytical methods give narrow transition band, flat passband and good stopband attenuation for a less filter order [14], [15]. Most methods do not allow independent control of band specifications, mainly the transition bandwidth. The lowpass filter designs can be extended to highpass, bandpass, and multiband FIR filters. In these filter designs center frequency and transition bandwidth can be easily varied. Thus tailor-made frequency response specifications can be obtained. The pulse shaping technique in [16] has features of high spectrum utilization efficiency, interference mitigation, flexible pulse length to meet the flexible data rate requirements, and good jitter resistant properties.

In [17], [18], [19], and [20], emphasis is given to the application of UWB radar technique for locating malignant breast tumors, where the backscattered signals are monitored by the placement of a set of antennas at specific locations on the breast. The pulses reflected by the tumor are received by probe antennas or antenna arrays placed at different locations. In monostatic UWB radar, the backscattered signals are collected by the transmitting antenna, with the antenna moved over the breast at various positions. The bistatic radar has a transmitting antenna and a receiving antenna placed at various positions. The multistatic radar has one transmitting antenna and several receiving antennas at various locations based on the design [19], [20], [21], [22], [23], [24]. Relatively large backscattered signals are produced in a localized region by malignant tumors because of the considerable difference in dielectric contrast between the malignant and normal breast tissue. The UWB radar system requires efficient antennas, and Vivaldi microstrip antenna is one which is widely used due to its features like wide impedance bandwidth, and gain [25], [26], [27], [28], [29], [30].

High-fidelity breast phantoms are crucial elements of simulation and experimental test bed for thoroughly examining and evaluating the efficacy of novel microwave breast cancer detection and treatment systems. Skin, adipose tissue (fat), and fibrous/connective/glandular (ductal and lobular) tissues are different tissue layers that make up the heterogeneous breast model. The ideal breast phantom that mimics the physical characteristics of tissues are important for microwave interactions with the phantom [31], [32]. Organs and tissues in the human body are identified by employing a segmentation procedure once a medical scan dataset is available [33]. A phantom is formed at the end of the segmentation process, which is further used in simulation software like Computer Simulation Technology Microwave Studio (CSTMWS). The University of Wisconsin, Madison, and the University of Calgary have published a large-scale dielectric spectroscopy investigation of malignant and healthy breast tissue at microwave frequencies, providing thorough information on the dielectric properties of normal and malignant breast tissue [34]. The knowledge of the dielectric properties helps the creation of numerical and physical high-fidelity breast phantoms. The human body contains tissues that exhibit frequency-dependent dispersive properties [35]. To incorporate the properties of an actual human breast model, it is necessary to accurately model the electromagnetic properties of human tissues [36]. The dielectric properties of biological tissues are represented using the Debye model. This model permits the representation of a wideband frequency-dependent dielectric spectrum through analytical representation [32]. The Cole-Cole model, which is a modified version of the Debye expression proposed in 1941,

is one of the most frequently employed models. It consists of four constant parameters similar to the Debye model and an additional exponent factor α [37].

When electromagnetic waves interact with biological tissues, they result in energy absorption, with a significant portion of the radiated power being absorbed by the breast tissues as the waves travel through the patient's breast from the transmitting antenna. The absorption per unit mass of the tissue can be estimated using SAR [38]. The potential risks associated with radiation exposure make it essential to limit the SAR induced inside the human breast by any microwave breast imaging system [39]. The SAR values used in this study are below the maximum standard SAR limit reported in [40], ensuring the safety of the proposed microwave breast cancer detection system. The distinction in dielectric properties between healthy and cancerous tissues results in variations in the absorption of incident microwave radiation, which can be measured by SAR. The absorption of Electro Magnetic (EM)radiation in cancerous tumors is higher than normal tissues, and therefore the maximum SAR value coordinates can be used to more accurately diagnose the position of the tumor in the breast [41]. For localizing tumors based on SAR, pulse shaping can enhance localization capabilities by mitigating the effects of reflections and multipath interference. UWB pulses with appropriate pulse shaping can achieve high precision and accuracy in detecting small changes in the electromagnetic properties of tissues, indicating tumor's presence. By decreasing the sidelobes and increasing the mainlobe of the UWB pulse, the accuracy of SAR-based tumor detection can be improved. Additionally, pulse shaping can reduce the peak power of the UWB pulse, which is a crucial consideration in SAR-based tumor detection since high peak power can cause tissue damage. By extending the duration of the pulse, the UWB pulse can achieve the same detection performance while minimizing the risk of tissue damage [42]. The SAR-based detection of breast cancer depends on various pulse features such as short pulse duration, which enhances the spatial resolution and reduces tissue scattering, high pulse repetition frequency (PRF), which improves the signal-to-noise ratio (SNR) and accuracy of breast cancer detection, low pulse rise time, which reduces frequency components outside the UWB bandwidth and potential interference affecting SAR measurements, low duty cycle, which limits SAR and reduces tissue heating, and an appropriate frequency range that enables optimal penetration into breast tissue while avoiding interference from other sources [43].

Recently, several image processing techniques utilizing machine learning (ML), artificial intelligence (AI), and neural network models have been implemented for detecting breast cancer. These systems are employed to improve the quality of images for human assessment and to automate the image analysis process to aid in better comprehension and interpretation. Numerous articles have been published on the detection, segmentation, and classification of breast cancer using ML and AI techniques [44]. Prior research has primarily focused on ML models using binary classification to identify specific cancers such as lung, brain, skin, stomach, kidney, and breast cancer. Analyzing complex biomedical data to extract biologically and diagnostically relevant features is a highly challenging task and plays a crucial role in detecting breast cancer using machine learning algorithms [45]. This challenge can be addressed by utilizing hybrid Machine Learning Classification Techniques incorporating ensemble techniques and an Enhanced-Grey Wolf Optimization (E-GWO) feature selection algorithm. This approach can significantly enhance the accuracy of predicting breast cancer [46]. One approach to improve accuracy for cancer detection is to use tools such as the Bayesian classifier-based wound characterization (BWC) technique, which can identify tumor-affected tissue with greater accuracy and facilitate early prognostic treatment for breast cancer [47].

The effect of UWB pulse shapes on accurate breast cancer detection is less investigated. Fewer pulse shaping techniques have been employed on Gaussian derivative pulses in the radar detection techniques for breast cancer detection. This had led to use of higher order derivatives of UWB pulses leading to increase in complexity and hence hardware for UWB generation to meet the requirements of FCC mask. Also, absence of pulse shaping leads to low SUE, less power concentration in the antenna mainlobe, which reduces the back scattered signals from small and deep-rooted tumors, making tumor detection difficult. The effect of UWB pulse shapes of different derivatives on the sensitivity and accurate detection of tumors of very small size at an early stage has to be investigated.

This paper proposes a pulse shaping technique for the source UWB seventh derivative pulse to excite the transmitter antenna of the bistatic and monostatic UWB radar mounted on the heterogeneous breast model. A band pass FIR filter is designed to spectrally modify the UWB pulse of center frequency 4 GHz. The resulting time and frequency domain analysis of backscattered signals for efficient tumor detection is carried out. The improvement in radiated power, radiation efficiency due to shaping technique employed and its impact on efficient tumor detection is examined. Finally, the effect of pulse shaping, on variations in back scattered signals, Scattering (S) parameter variations and electric field intensity variations for deeply rooted tumor is discussed. Also, SAR analysis employing monostatic radar is carried out on the heterogeneous and homogeneous breast model to locate the position of tumor. Experimental validation of the proposed system is performed by employing artificial heterogeneous breast phantom fabricated based on [48] and monostatic radar. The breast phantom closely mimics the dielectric properties of actual breast tissues. The experimental validation process involves measuring the scattering parameter S11 response of the antenna radiating parallel to the artificial breast phantom embedded with a

4 mm diameter tumor. Variations in the scattering parameter values indicates the presence of the tumor within the breast, making it a promising option for clinical trials.

The work has following major contributions:

- A shaping technique is proposed, employing the sharp transition bandpass FIR filter, to shape the source UWB seventh derivative Gaussian pulse. The shaped pulse excites the antenna of the bistatic and monostatic UWB radar system mounted on the Cole Cole breast model for tumor detection.
- The shaped UWB pulse compliance with FCC spectral mask specifications to achieve higher spectral utilization efficiency and meet the safety standards of signal transmission through the breast and its impact on accurate detection of small sized tumor.
- Time and frequency domain analysis of backscattered UWB signals from the tumor for efficient tumor detection.
- The effect of pulse shaping on finding the exact location of the tumor by identifying the coordinates of the maximum value of SAR for different tumor sizes, locations and frequencies.
- Investigation of trade-off between signal penetration depth and tumor spatial resolution with signal center frequency in homogeneous fibroglandular layer.
- The proposed breast tumor detection technique is experimentally validated using fabricated heterogeneous breast phantom with monostatic radar system.

The rest of the paper is organized as follows: The numerical breast phantom Cole-Cole model, tumor dielectric properties and chemical composition has been presented in section II. UWB monostatic and bistatic radar setup for breast tumor detection and the proposed pulse shaper design employing bandpass filter have been discussed in Section III. In section IV, experimental setup of the proposed tumor detection technique for fabricated breast phantom using monostataic radar technique is discussed. In section V, the simulations carried out, and experimental validations are discussed. Amplitude variations of backscattered signal from the tumor, S parameter variations, and electric field intensity variations are analysed to illustrate the usefulness of the proposed pulse shaping technique for breast cancer detection. SAR analysis is carried out to identify the tumor's precise location. Also, the effect of variations in the center frequency of shaped UWB signal on the depth of penetration of UWB pulse and tumor location accuracy in fibroglandular layer are investigated. Finally, Section VI gives the concluding remarks and future work.

II. BREAST MODEL AND TUMOR

Several anatomically accurate numerical breast phantoms created from Magnetic Resonance Imaging (MRI) are available in the University of Wisconsin Cross-Disciplinary Electromagnetics Laboratory (UWCEM) repository for the detection and treatment of breast cancer. The breast tissues in these phantoms have realistic ultrawideband dielectric characteristics of normal breast tissue from 0.5 GHz to 20 GHz, as reported in [31] and [32] and represent the structural heterogeneity of normal breast tissue. Breast phantoms are created by utilizing a sequence of T1-weighted MRIs taken from patients in prone position. These phantoms comprise a three-dimensional grid of cubic voxels, each measuring 0.5mm x 0.5mm x 0.5mm. The breast model is made up of a skin layer that is about 1.5mm thick, a subcutaneous fat layer at the base of the breast that is 1.5cm thick, and a muscle chest wall that is 0.5cm thick [31]. The phantom used in this research is developed based on the ultrawideband dielectric properties of 155 normal, cancerous, and benign breast tissue samples ranging from 0.5-20 GHz. These tissue samples were obtained from cancer surgeries at the University of Wisconsin and the University of Calgary hospitals, as reported in [31] and [32]. This closely mimics a realistic phantom and is expected to be highly accurate which is numerically represented as Cole-Cole model. This model is employed in CSTMWS.

TABLE 1. Cole-Cole parameters for female breast tissue.

Tissue Type	ε_s	ε_∞	τ	α (ps)	σ
Skin	37	4	7.37	0.06	1.10
Fat	16.29	6.57	7.23	0.09	0.23
Fibroglandular	35.14	5.28	7	0.06	0.46
Tumor	54	4	7.23	0.07	0.7

This paper utilizes a single-pole Cole-Cole model based on the measurements to represent the complex relative permittivity. The dielectric constant $\varepsilon(\omega)$ of a bio-layer is derived by the Cole-Cole model, given by (1) [37].

$$\varepsilon(\omega) = \varepsilon'(\omega) - j\varepsilon''(\omega) = \varepsilon_\infty + \frac{\varepsilon_s - \varepsilon_\infty}{1 + (j\omega\tau)^{1-\alpha}} + \frac{\sigma}{j\omega\varepsilon_0} \quad (1)$$

In the given equation, the real and imaginary parts of the complex relative permittivity are denoted by ε' and ε'' respectively and vary with the angular frequency ω. The static permittivity is denoted by ε_s, and the high-frequency permittivity is represented by ε_∞. The relaxation time constant is indicated by τ, while α is the parameter that broadens the dispersion. The static conductivity is denoted by σ. The table 1 displays the first Cole-Cole parameters for female breast tissue.

Cancerous cells have more water content than normal cells. The water content present in the tissue has a significant effect on the dielectric properties of the tissue. The potassium concentration is high, and that of sodium is low for healthy cells in the human body. Cancerous cells have changes in membrane potential and capacitance due to differences in the membrane composition and abnormalities in the energy and charge distribution. Compared to healthy cells, cancerous cells have lower membrane potential due to the flow of water into the cells and the movement of minerals like zinc, potassium, magnesium, and calcium out from the cell interior [49]. Low membrane potential of cancerous cells, when compared to healthy cells, is also due to an increase

in intracellular concentration of positively charged sodium ions and negative charges on cell coat i.e., glycocalyx. Low membrane potential causes lower intensities of electric field in cancerous tissues compared to normal tissues. The relative robustness of normal cells and the sensitivity of malignant cells to the application of an electric field demonstrate greater efficacy of electrochemotherapy utilising lower medication concentrations like lower electric field strength of cancerous cells compared to normal cells making them more susceptible to electrical pulse mediated drug delivery. Results from the field analysis could be utilised to decide the best parameters for treating tumor tissues [50].

III. UWB RADAR FOR BREAST TUMOR DETECTION

UWB radar employed in this setup has a transmitting and receiving antenna placed at predetermined positions on the breast. The transmitted signal hits the tumor of the breast phantom model, and the backscattered signals from the malignant tissue are collected by the receiver antenna resulting in localized regions of relatively large backscattered energy, which aids in detecting the presence of the tumor.

A. PULSE SHAPER FOR UWB SOURCE SIGNAL

In this work, the transmitter antenna of UWB radar system is excited with a seventh derivative Gaussian pulse which is further shaped using the FIR bandpass filter. The UWB seventh order Gaussian pulse is (2) [51].

$$g(t) = K\left(\frac{105t}{\sigma_1^8} - \frac{105t^3}{\sigma_1^{10}} + \frac{21t^5}{\sigma_1^{12}} - \frac{t^7}{\sigma_1^{14}}\right)e^{\left(\frac{-t^2}{2\sigma_1^2}\right)} \quad (2)$$

where σ_1 is the Gaussian Pulse Shaping Factor (PSF) and K is scaling coefficient. Gaussian pulse is used for pulse transmission through the human body for IR-UWB systems with desired center frequency and frequency band [52]. Digital FIR filters are employed to control the spectral shape of the UWB pulses. They maximize the resultant transmit power and also match the FCC mask. Sharp transition FIR filters [14], [15] are synthesized to obtain a narrow transition band and good stopband attenuation with less filter order L. Also, variable center frequency and passbands as per FCC mask specifications required for this application are achieved. The closed form expression is obtained for impulse response coefficients.

In the proposed sharp transition bandpass FIR filter design, the desired frequency response $H_d(j\omega)$ is modelled based on the required FCC mask specifications of desired bandwidth and centre frequency of the UWB pulse as shown in Fig. 1. The modelling is done to reduce Gibb's phenomenon by employing suitable trigonometric functions.

Further, employing the frequency sampling technique, the model frequency response is sampled and the filter coefficients are obtained. The objective is to obtain a sharp roll off with the least filter length L. By evaluating the integrals, the impulse response coefficients $h(n)$ of the filter

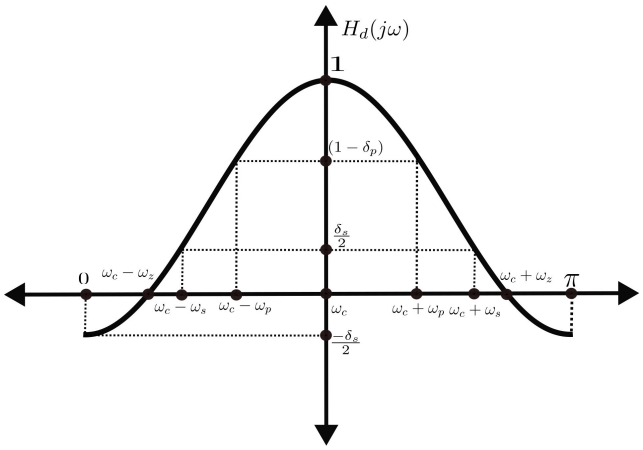

FIGURE 1. Frequency response model of UWB pulse shaping filter for FCC mask compliance.

are obtained as (3).

$$\begin{aligned} h(n) &= \int_0^{\omega_c-\omega_z} \left(\frac{-k_{ps}\delta_s}{2}\left(1-\cos\left((\omega_c-\omega_z)-\omega\right)\right)\right)\cos(k\omega)d\omega \\ &+ \int_{\omega_c-\omega_z}^{\omega_c-\omega_p} (1-\delta_p)\cos\left(k_{pt}\left((\omega_c-\omega_p)-\omega\right)\right)\cos(k\omega)d\omega \\ &+ \int_{\omega_c-\omega_p}^{\omega_c} \left(\cos\left(k_{pp}(\omega_c-\omega)\right)\right)\cos(k\omega)d\omega \end{aligned} \quad (3)$$

where $n = 0, 1, \ldots, \frac{L-1}{2}$ for L odd, $k = \frac{L-1}{2} - n$, ω_p is the pass band frequency, $H(\omega) = 0$ at ω_z, ω_c is the center frequency, δ_p is the 3dB passband, δ_s is the dominant side lobe level, k_{pp}, k_{pt}, and k_{ps} are the parameters derived based on the magnitude response model which shape the response in the passband, transition band, and stopband respectively [12], [34]. The shaped UWB pulse is fed to the antenna and transmitted through the body is obtained as (4), where T is the sampling interval.

$$P(nT) = \sum_{n=0}^{L-1} h(n)g(t-nT) \quad (4)$$

B. BISTATIC UWB RADAR SETUP

The bistatic UWB radar system is simulated using CST MWS, as shown in Fig. 2. It has two vertical endfire Vivaldi microstrip antennas touching the hemispherical model of the breast with a spatial separation angle of 90^0. One antenna is a transmitter, and the other is a receiver. The Vivaldi microstrip antennas of size $45mm \times 40mm$ with a wide bandwidth ranging from 3-10 GHz are employed to suit the desired specifications [22]. The transmitter antenna is excited with the shaped seventh derivative Gaussian pulse with a center frequency of 4 GHz. The tumor is located at depth of 5.5cm from the skin layer at coordinates in (mm) [0,5,0].

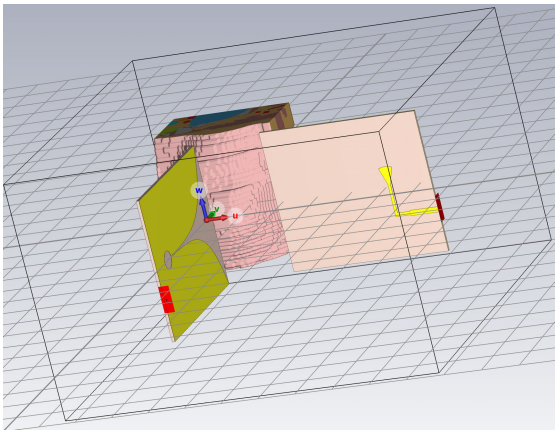

FIGURE 2. CST simulation set up of bistatic UWB radar for tumor detection on Cole-Cole breast phantom model with vertical endfire orthogonal transmitting and receiving antennas.

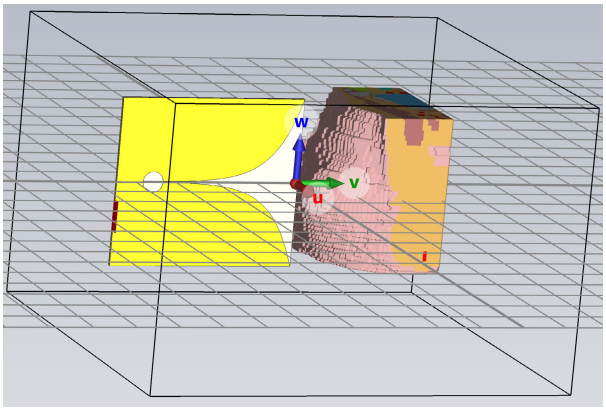

FIGURE 3. CST simulation set up of mostatic UWB radar for tumor detection on Cole-Cole breast phantom model based on SAR.

C. MONOSTATIC UWB RADAR SETUP FOR SAR ANALYSIS

SAR is used to detect abnormalities in human breast tissue by measuring the energy absorbed by biological tissues from electromagnetic waves. This results in localized regions of high specific absorption rate that aid in detecting the presence and location of the tumor. This absorption causes heating of the tissue, which can be quantified by SAR. Therefore, the focus is on the area where maximum absorption occurs due to the presence of a tumor. This approach demonstrates the usefulness of using maximum SAR value coordinates to detect the tumor position in the breast. The absorbed power is measured for a normal breast and breast with tumor. The maximum value of SAR is also analyzed at different tumor locations and various frequency ranges. The expression of SAR is given by (5).

$$SAR = \frac{\sigma \vec{E}^2}{\rho} \tag{5}$$

where $\vec{E}$ electric-field in (V/m), σ is the conductivity in (S/m) and ρ is the tissue density in kg/m^3.

FIGURE 4. Fabricated heterogeneous breast phantom with tumor in a mould with skin (green), fat (yellow), gland (red), and tumor (blue) layers.

In this setup, a monostatic radar is used, which employs a single UWB antenna that acts as both transmitter and receiver. As shown in the Fig. 3, the monostatic radar is placed on the breast model. The transmitter is excited with the pulse obtained from the designed pulse shaper. The transmitted signal hits the tumor of the breast phantom model, and the backscattered signals from the malignant tissue are collected by the same antenna. SAR is used to detect abnormalities in human breast tissue by measuring the energy absorbed by biological tissues from electromagnetic waves. This results in localized regions of high specific absorption rate that aid in detecting the presence and location of the tumor. The maximum SAR coordinates indicate the location of tumor.

IV. EXPERIMENTAL SETUP FOR BREAST CANCER DETECTION

A. HETEROGENEOUS BREAST PHANTOM FABRICATION

For experimental validation of proposed technique, a heterogeneous breast phantom is fabricated as shown in Fig. 4. The chemical composition of each layer is listed in Table 2 and its electrical properties are shown in shown in Table 3 [48].

B. EXPERIMENTAL SETUP

Fig. 5 shows the experimental setup consisting of heterogeneous breast phantom and monostatic radar system for breast cancer detection. It consists of Vivaldi antenna excited by the shaped UWB pulse with a center frequency of 4 GHz and connected to the Keysight Vector Network Analyzer (VNA) E5063A in the anechoic chamber. Antenna is placed parallel to the breast phantom to radiate signal into the breast and the backscattered signal from the phantom are collected by the same antenna.

TABLE 2. The composition of heterogeneous breast phantom [48].

Material	Quantity			
	Skin	Fat	Gland	Tumor
Distilled water	80 ml	40 ml	80 ml	100 ml
Safflower oil	14 ml	39 ml	21 ml	7 ml
Propylene glycol	7 ml	2 ml	7 ml	6.5 ml
Agar agar - gelatin powder	5.88 g	7 g	5 g	9 g
Formalin (37% formaldehyde solution)	0.30 ml	0.30 ml	0.30 ml	0.30 ml
Xanthan gum	1.3 g	1.3 g	1.3 g	1.3 g
Liquid detergent	0.30 ml	0.30 ml	0.30 ml	0.30 ml

TABLE 3. Electrical properties of breast phantom [48].

Layer description	Dielectric constant ε_r	Conductivity (σ in S/m)
Skin layer	23.44	2.49
Fat layer	5.75	1.72
Fibroglandular layer	15.75	3.27
Tumor	40.57	4.98

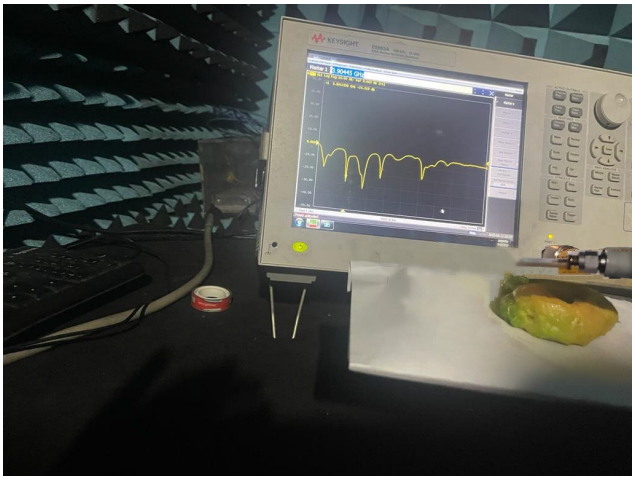

FIGURE 5. Experimental set up of monostatic UWB radar for tumor detection employing heterogeneous fabricated breast phantom.

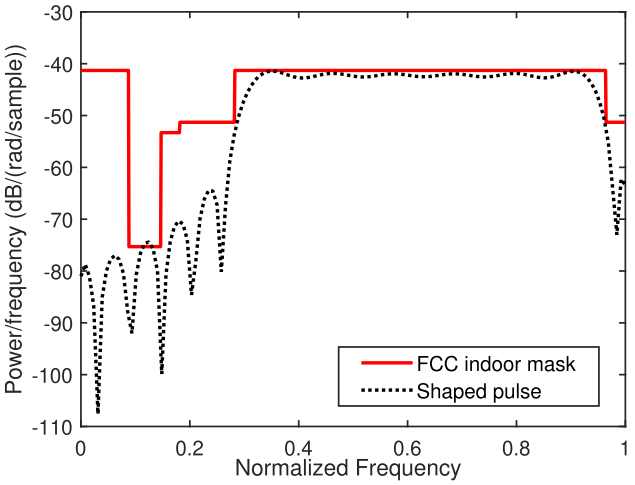

FIGURE 6. Spectral mask of FCC and PSD of shaped UWB pulse employing proposed pulse shaper for frequency band 3.1-10.6 GHz.

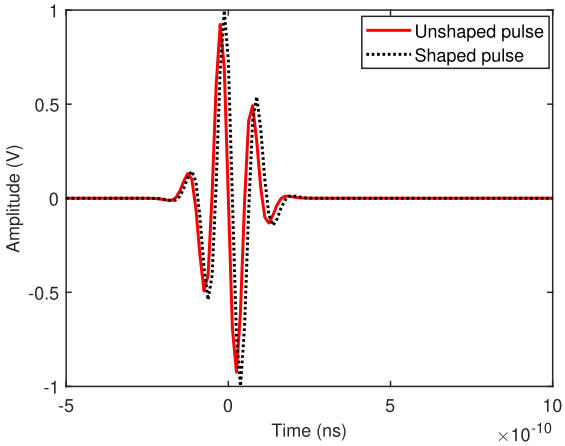

FIGURE 7. Time domain shaped and unshaped seventh derivative Gaussian UWB pulse of width 0.4 ns fed to the Vivaldi antenna of the radar system.

V. RESULTS

A UWB radar based breast cancer detection system is implemented. The proposed shaped seventh derivative Gaussian pulse is used to excite the transmitter antenna of bistatic UWB radar. UWB pulses are tailored to comply with the FCC mask varying from the range 3.1-10.6 GHz, encompass the medical band of 3.4-4.8 GHz, and satisfy the Power Spectral Density (PSD) limited to -41.3 dBm/MHz for UWB pulse propagation through the human body [53]. It is observed from Fig. 6 that the shaped UWB pulse fit within the FCC properly. Good spectral utilization efficiency of 84% is achieved. Thus, most of the power is within the frequency band desired. This is possible due to bandpass pulse shaper design which allows desired flexible passbands and stopbands to fit the FCC mask.

Fig. 7 shows the shaped Gaussian pulse obtained employing proposed sharp transition bandpass filter. It has higher amplitude due to pulse shaping and low ringing oscillations that will increase antenna power distribution. Also, a sharp pulse is obtained of pulse width 0.4 ns, thus achieving a higher data rate and precise location detection of tumor.

The frequency response of the shaped pulse obtained by employing the proposed pulse shaping filter with center frequency of 4 GHz with length 15, has a sharp mainlobe, low dominant SLL, and drooping sidelobe characteristics with First Null to Last Null ratio of 0.8, as seen in Fig. 8 which reduces interference issues during pulse propagation through the human body.

Fig. 9 shows that the radiated power from Vivaldi antenna excited by the shaped seventh derivative Gaussian pulse achieves 3.63 milliwatts more radiated power compared to the pulse without shaping. This ensures higher reflected power,

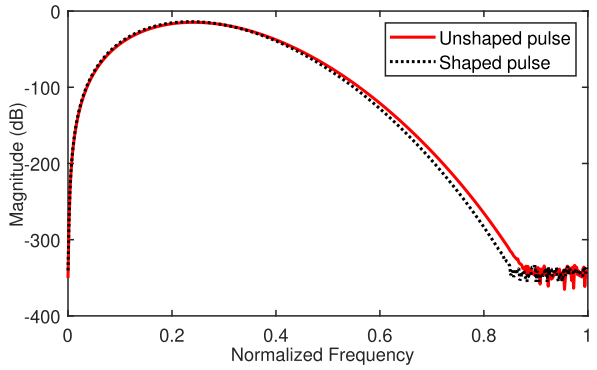

FIGURE 8. Frequency response of shaped and unshaped seventh derivative UWB Gaussian pulse.

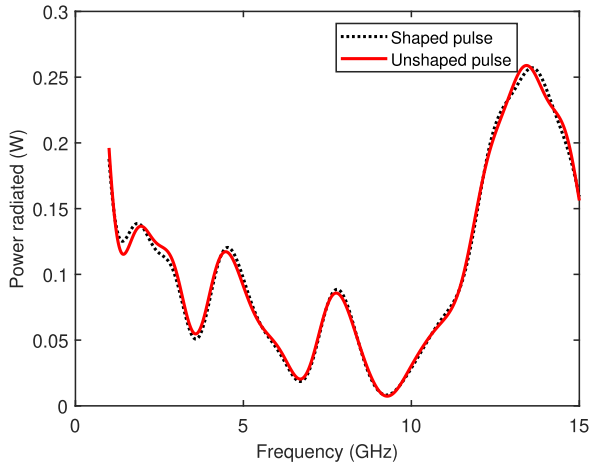

FIGURE 9. Antenna radiated power for seventh derivative Gaussian pulse with and without shaping.

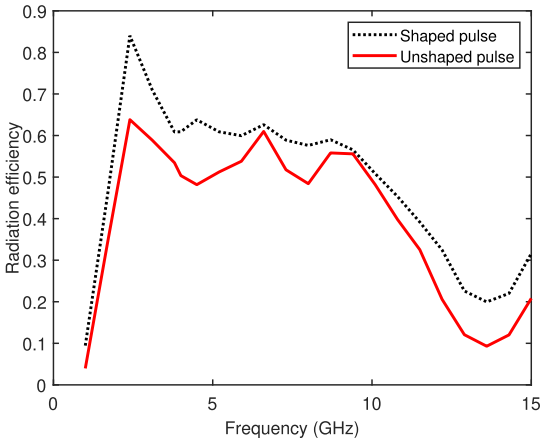

FIGURE 10. Radiation efficiency of the UWB Vivaldi antenna excited with shaped and unshaped seventh derivative UWB Gaussian pulse.

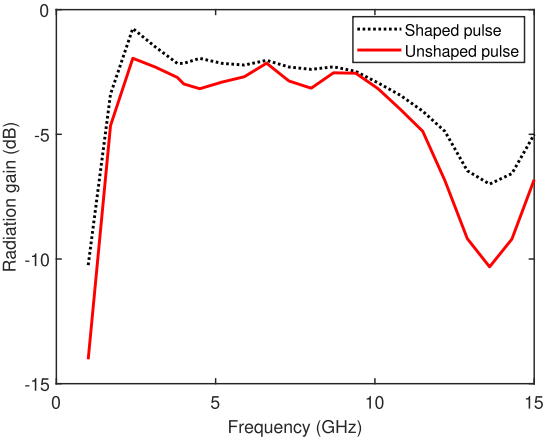

FIGURE 11. Antenna radiation gain with unshaped and shaped seventh derivative UWB Gaussian excitation pulse.

i.e. backscattered signals from the tumor location that helps to detect tumor accurately. Also, it ensures the option to select less source power signal transmission through the body for the safety of the patient.

Fig. 10 and Fig. 11 show that the radiation efficiency and gain when excited by the shaped seventh derivative Gaussian pulse are 61.02% and −2.14dB, respectively and unshaped pulse values are 50.25% and −2.988dB respectively, at 4 GHz frequency. The radiation gain and efficiency are better than in [54] due to the concentration of more power in the main lobe and suppression of sidelobes in the proposed design. This implies that a shaped pulse can penetrate deeper into different layers of breast compared to Gaussian pulses without shaping.

The far field directivity plot shown in Fig. 12 shows that the transmitting Vivaldi antenna has a gain of 5.44 dBi, and half power beamwidth of 65.2^0. This ensures wide coverage of radiated power over the breast surface for detection of tumor based on backscattered signals and mitigation of interference issues due to low Side Lobe Level (SLL) of −4.7 dB as compared to a gain of 5.32 dBi, beam width of 65.5^0 and SLL of −4.6 dBi for the unshaped pulse.

Fig. 13 shows the signal propagation through different layers of the breast for the shaped and unshaped Gaussian pulse. It is seen that attenuation is less for shaped signals, thus providing higher transmission power. Hence, for the shaped seventh derivative UWB pulse, the maximum amplitude of the electric field at the tumor location is 22.56 V/m, and at air skin interface is 24.52 V/m, whereas these values are 20.98 V/m and 21.53 V/m respectively for unshaped pulse.

In Fig. 14 and Fig. 15, the amplitude variation of peak voltage indicates the presence of 4 mm and 2 mm tumor, respectively. The dielectric contrast between malignant and normal breast tissue is 5:1 [49].This has resulted in higher backscattered energy from the tumor location as observed in Fig. 14 and Fig. 15. The tumor detection can be observed from 0.9124 ns to 0.9134 ns of the received signal with an amplitude higher than [18], as shown in Fig. 14 and Fig. 15. Variations in phase shift is also observed for the backscattered signals from the tumors when superimposed over the backscattered signals from a normal breast.

Table 4 shows that the peak amplitude of the backscattered signal is constant for normal breast without tumor, amplitude

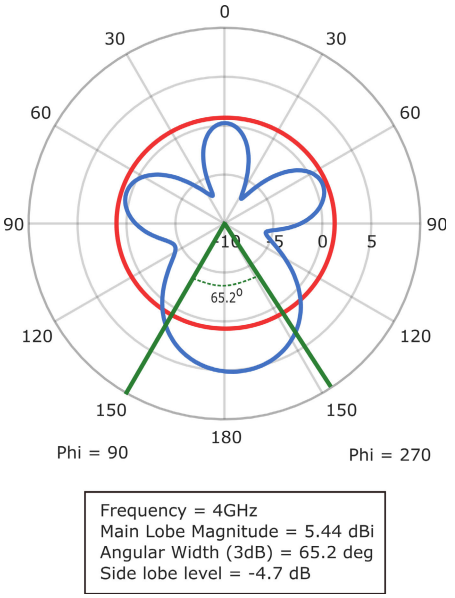

FIGURE 12. Far field directivity of transmitting antenna excited by shaped Gaussian pulse.

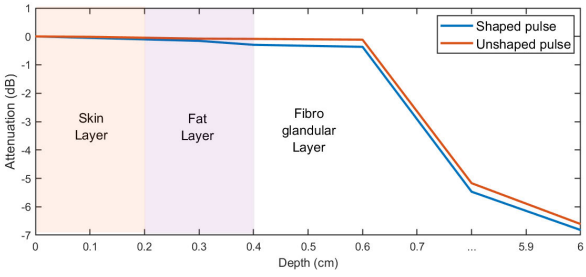

FIGURE 13. UWB signal attenuation at various layers of the breast for shaped and unshaped UWB pulse at 4 GHz.

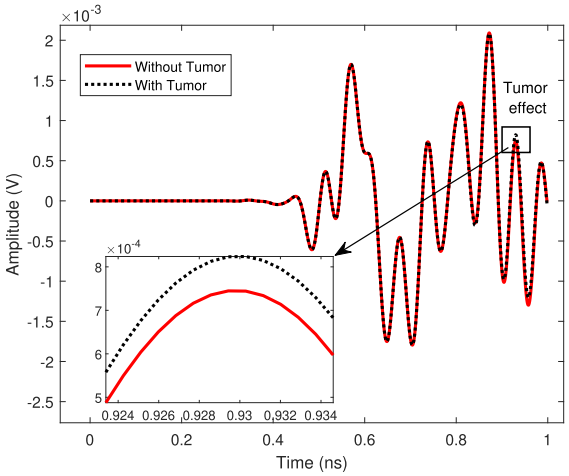

FIGURE 14. Amplitude variations of backscattered UWB signals without and with tumor of 4 mm radius at a depth of 4 cm from the skin layer.

of the backscattered signal is more when the tumor radius is 4 mm, and the amplitude reduces as the tumor radius decreases to 2 mm, 1 mm, and 0.5 mm. It is observed from

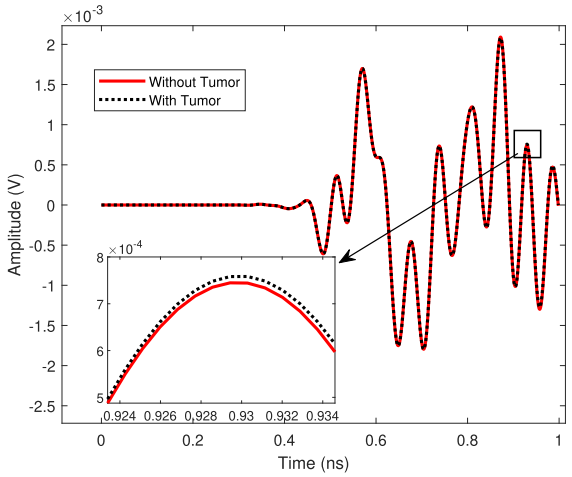

FIGURE 15. Amplitude variations of backscattered UWB signals without and with tumor of 2 mm radius at a depth of 4 cm from the skin layer.

the Table 4 that for 0.5mm tumor, the amplitude variations are very less.

Table 5 shows tumor located at various depths to determine the reach of transmitted signals through the breast. Signal upto a depth of 5.5 cm and tumor size of 4 mm could be detected using the shaped signal for the given signal power.

Fig. 16 and Fig. 17 show scattering parameter plots of S11 and S21 with a tumor of 4mm radius is shifted upwards when compared to the normal breast. It is observed that the frequency band of 3.4-4.6 GHz shows more signal reflection hence detects the presence of tumor in the breast phantom, as also seen in [18].

In Fig. 18, it is observed that for a frequency of 4 GHz and tumor radius of 2 mm, the received signal is reduced due to lesser backscattering of signal from the tumor as a result of reduction in tumor radius. Table 6 shows that the electric field intensity at the tumor location and at air skin interface is more for the shaped signals compared to without shaping signal, due to more energy content associated with shaped signals. Fig. 19 and Fig. 20 show the variations in the electric field versus time and frequency, respectively, for normal breast and the breast with tumor of radii 4mm, 2mm, and 1mm. The cancerous tissues have much lower electric field strength compared to normal cells. The reduction is due to the altered membrane composition and permeability due to the movements of minerals like potassium, sodium, calcium, and magnesium [49]. Higher electric field intensity amplitude variation is observed in the proposed technique for tumor breast which aids in detection, compared to [50].

Fig. 21 shows the comparison plot of antenna S11 parameters with and without tumor for experimental validation. The Vivaldi antenna is positioned parallel to a breast phantom that includes a tumor. Notable reflections are detected in the S11 parameter measurements within the frequency range of 3.6-5.4 GHz. These deviations arise from the disparities in dielectric properties between healthy breast tissues and those affected by tumors. The higher water content within the tumor

TABLE 4. Peak voltage variations of backscattered signals between normal and breast with tumor for various tumor radii.

Peak voltage of normal breast	Peak voltage difference			
	4 mm tumor	2 mm tumor	1 mm tumor	0.5 mm tumor
0.01348 V	0.00132 V	0.000355 V	0.00004 V	0.00002746 V

TABLE 5. Backscattered signals at UWB radar receiver for various depths from the skin layer for 4mm size tumor.

Peak voltage				
Normal breast	4 cm	4.5 cm	5cm	5.5 cm
0.01348 V	0.01480 V	0.0137 V	0.01353 V	0.01347 V

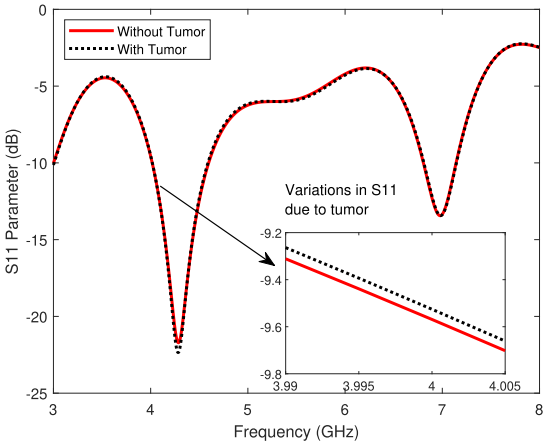

FIGURE 16. S11 plot of bistatic UWB radar mounted on the breast, excited by the shaped seventh derivative Gaussian UWB pulse without and with tumor of 4 mm radius.

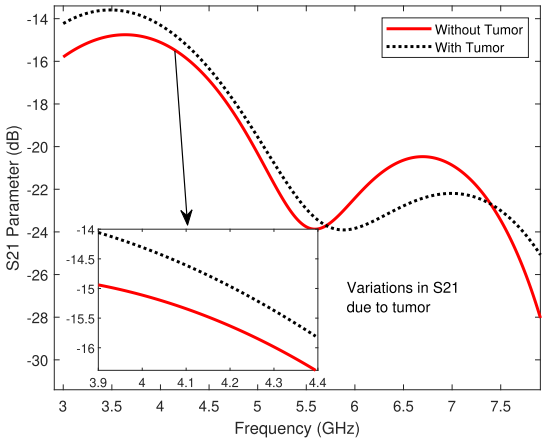

FIGURE 17. S21 plot of bistatic UWB radar mounted on the breast, excited by the shaped seventh derivative Gaussian UWB pulse without and with tumor of 2 mm radius.

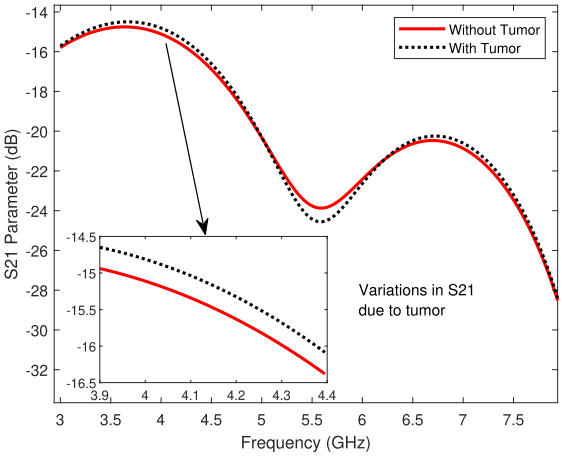

FIGURE 18. S21 plot of bistatic UWB radar mounted on the breast, excited by the shaped seventh derivative Gaussian UWB pulse without and with tumor of 2 mm radius.

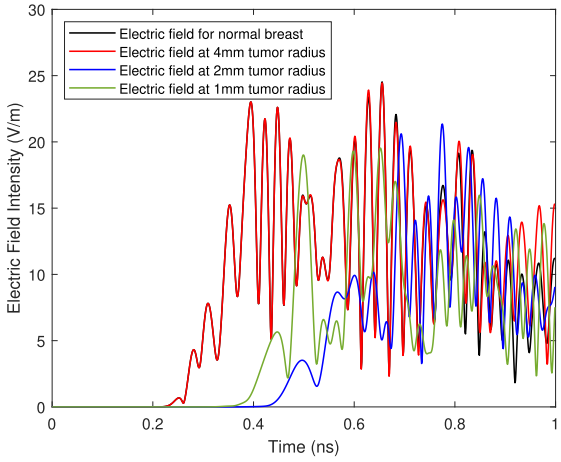

FIGURE 19. Time behaviour of shaped seventh derivative Gaussian pulse incident on the breast without and with tumor of radii 4 mm, 2 mm, and 1 mm.

cells plays a key role in the contrasting electrical properties of the breast tissues, leading to an increased number of reflections in the S11 parameter plot of the antenna when interacting with the region affected by the tumor.

Analysis of average SAR is carried for the heterogeneous breast phantom. The shaped UWB pulse using the proposed pulse shaper illuminates heterogeneous breast phantom using monostatic radar mounted on it. The resonant frequency of 3, 4, and 5 GHz result in the highest SAR with coordinates of maximum SAR. In Table 7, the total SAR, maximum SAR, and coordinates of maximum SAR values are given for a heterogeneous breast phantom without a tumor when 10 g analysis was carried out. Similarly, Table 8 provides these values for a breast phantom with tumor of radius 4 mm having (0, 5, 0) mm as the coordinates of the location. By comparing the coordinates values of maximum SAR of the heterogeneous breast phantom with and without tumor at various frequencies, it can be observed that as the frequency increases, the coordinates values of maximum SAR are very close to the coordinates of actual tumor location

TABLE 6. Electric field intensity and channel loss for various tumor radii in heterogeneous breast model.

Electric field (V/m)				At air skin interface (V/m)			Channel loss in dB at tumor for 4 GHz		
Tumor radius	4 mm	2 mm	1 mm	4 mm	2 mm	1 mm	4 mm	2 mm	1mm
Shaped UWB pulse	22.56	21.34	19.53	24.52	24.52	24.52	-0.723	-1.206	-1.976
Unshaped UWB pulse	20.98	19.53	18.51	21.53	21.53	21.53	-0.224	-0.846	-1.31

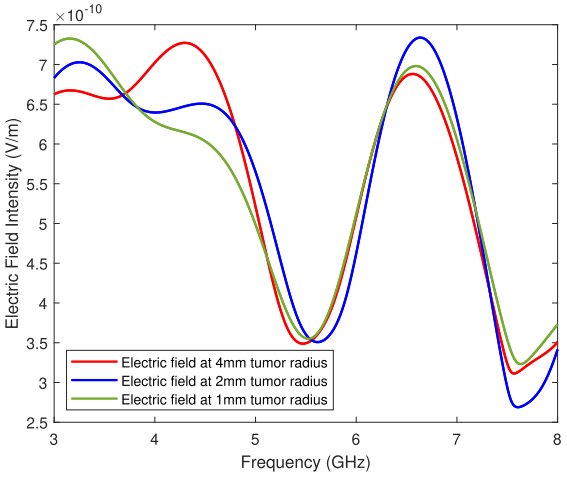

FIGURE 20. Spectrum behaviour of shaped seventh derivative Gaussian time pulse incident on the breast without and with tumor of radii 4 mm, 2 mm, and 1 mm.

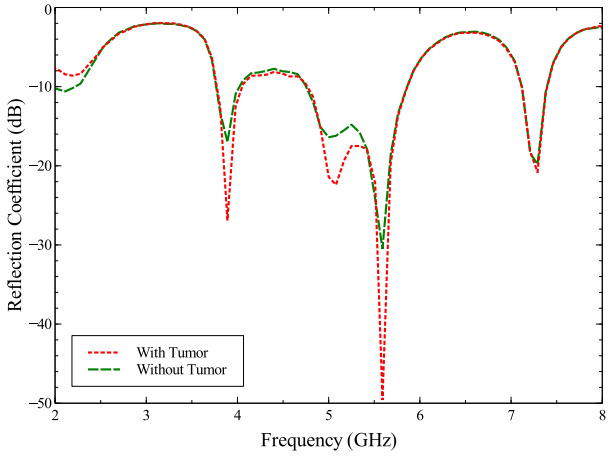

FIGURE 21. Measured reflection coefficient S11 obtained for the experimental setup consisting of fabricated breast phantom with and without tumor and monostatic radar system.

TABLE 7. SAR average in 10 g tissue and co-ordinates of maximum SAR in the heterogeneous breast model without tumor.

Frequency (GHz)	10 Gram Analysis		
	Maximum SAR WKg^{-1}	Total SAR WKg^{-1}	Maximum SAR at (x,y,z) mm
3	0.845	0.432	0.21,14.34, 2.34
4	1.31	0.865	-0.21,19.45, 4.56
5	0.643	0.231	0.21,16.21, 6.54

TABLE 8. SAR average in 10 g tissue and coordinates of maximum SAR in the heterogeneous breast model with tumor of radius 4 mm located at (0,5,0) mm co-ordinates.

Frequency (GHz)	10 Gram Analysis		
	Maximum SAR WKg^{-1}	Total SAR WKg^{-1}	Maximum SAR at (x,y,z) mm
3	2.72	0.956	-0.21,4.1, -0.75
4	2.61	1.28	0.21,4.3,0.85
5	2.41	0.986	0.21,4.5,-0.53

TABLE 9. SAR average in 10 g tissue and coordinates of maximum SAR in the heterogeneous breast model with tumor of radius 4 mm located at (0,5,0) mm co-ordinates at 4 GHz for shaped and unshaped pulse.

Parameters	10 Gram Analysis	
	Shaped pulse	Unshaped pulse
Maximum SAR value	2.61 W/kg	2.314 W/kg
Maximum SAR coordinates (x,y,z) in mm	-0.21,4.3,-0.75	-0.21,4.3,-0.75
Total SAR value	1.28 W/kg	0.96W/kg

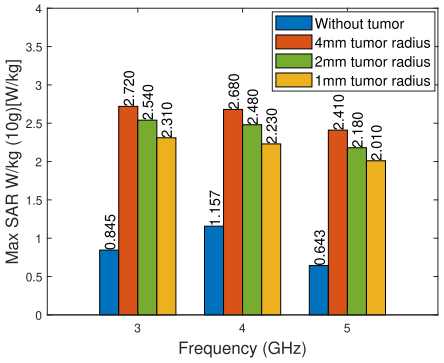

FIGURE 22. Comparison of maximum SAR value for various frequencies in the breast with and without tumor.

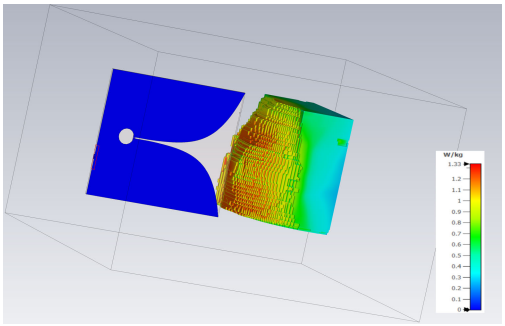

FIGURE 23. Maximum SAR for the heterogeneous breast model without tumor at 4 GHz.

i.e. (0, 5, 0) mm as seen in Table 8. It is evident from Fig. 22 that the maximum SAR is consistently higher in the breast phantom with a tumor than in the one without a tumor at all three frequency ranges. Maximum SAR value

TABLE 10. SAR and co-ordinates of maximum SAR with variation in depth and frequency in homogeneous fibroglandular layer with tumor at a depth of 12 mm and 14 mm i.e. at co-ordinates (0, 0, 12) mm and (0, 0, 14) mm respectively.

Tumor Radius	Depth	Maximum SAR (W/kg)			Maximum SAR at (x,y,z) mm.		
		3.5 GHz	4 GHz	4.5 GHz	3.5 GHz	4 GHz	4.5 GHz
4 mm	12mm	0.709 W/kg	0.509 W/kg	0.443 W/kg	(0.0791,-0.9390,9.9667)	(0.0791,-0.939,9.966)	(0.0791,0.3,11.263)
	14 mm	0.700 W/kg	0.496 W/kg	0.436 W/kg	(0.0791,-0.9390,9.9667)	(0.0791,-1.107,9.921)	(0.0791,0.3,14.283)
2 mm	12 mm	0.703 W/kg	0.501 W/kg	0.432 W/kg	(0.0791,-0.9390,9.9667)	(0.0791,-1.107,9.625)	(0.0791,0.3,11.058)
	14 mm	0.701 W/kg	0.494 W/kg	0.434 W/kg	(0.0791,-0.9390,9.9667)	(0.0791,-1.107,9.401)	(0.0791,0.3,14.369)

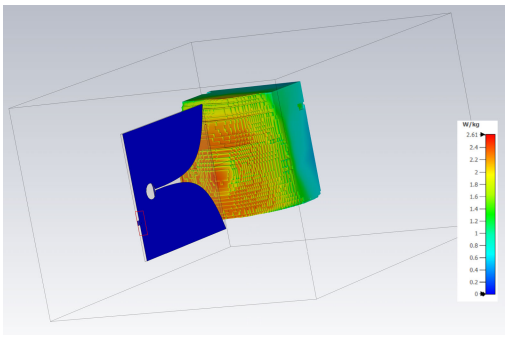

FIGURE 24. Maximum SAR for the heterogeneous breast model with 4 mm tumor at 4 GHz.

obtained after the simulation of monostatic radar setup in CSTMWS for the heterogeneous breast model without and with 4mm tumor at 4 GHz is shown in Fig. 23 and Fig. 24 respectively. This finding clearly indicates the presence and location of the tumor. Table 9 compares total SAR and maximum SAR values when shaped and unshaped pulse is employed for tumor detection in monostatic radar setup. It is observed that the SAR value for the shaped UWB pulse is more than unshaped UWB pulse due to higher electric field at the tumor location. From Table 10, it is observed that increase in the center frequency of UWB pulse when penetrating through homogeneous fibroglandular layer, the penetrated electric field and hence maximum SAR value reduces due to the absorption of signal energy by the tissues of the breast. Also, its shorter wavelength enables better discrimination and localization of small abnormalities within the fibroglandular layer, enhancing the spatial resolution of tumor. Thus, an increase in the frequency can lead to decreased SAR and improved spatial resolution as observed from maximum SAR and coordinate values of maximum SAR in Table 10. Table 11 shows that the shaped pulse, due to its higher radiating efficiency, has higher energy content and hence has a higher penetrated electric field compared to an unshaped UWB pulse for any depth and frequency. This allows a higher frequency pulse to be employed for better spatial resolution of small-size tumor locations. Also, a higher electric field due to the shaped pulse aids in detecting deep-rooted tumors. Observing Tables 10 and 11, optimizing the spatial resolution and penetration depth with frequency is necessary for effective breast cancer detection. Based on both the simulation and experimental study conducted, it is observed that frequency band 3.6-5.4 GHz is most effective

TABLE 11. Penetrated electric field intensity in homogeneous fibroglandular layer with variations in depth and frequency for shaped and unshaped UWB pulse.

Frequency	Depth	Maximum electric field (V/m)	
		Unshaped UWB pulse	Shaped UWB pulse
3.5 GHz	12 mm	16.77 V/m	35.76 V/m
	14 mm	14.32 V/m	27.32 V/m
4 GHz	12 mm	12.46 V/m	33.47 V/m
	14 mm	11.52 V/m	26.73 V/m

for the breast phantom considered in the study and to achieve best trade-off between penetration and spatial resolution of the tumor. Also results of experimental study conducted closely match with the simulation results.

VI. CONCLUSION

This paper presents a UWB radar-based breast tumor detection technique with a time and frequency domain analysis. This paper emphasizes the source UWB signal employed to excite the Vivaldi antenna of the UWB radar system mounted on the breast phantom. The source seventh order Gaussian pulse is shaped using the proposed bandpass pulse shaper. The proposed technique obtains the optimal filter coefficients for shaping the UWB pulse to fit FCC mask specifications with low filter length. The pulse shaper filter design has a higher roll-off rate, hence suitable for very short duration sharp UWB pulse shaping, achieves higher data rate, less interference issues, and low ringing effect. Thus, improved antenna power distribution and location accuracy of tumors are observed. Simulation results show higher variations in the amplitude of the received signal with tumor and S parameter values due to higher radiated power produced by the shaped pulse. The shaped UWB pulse propagated through different layers of the breast has reduced channel loss and higher radiated efficiency for various frequencies. The higher energy content with a shaped pulse results in higher electric field intensity variations, even for a smaller-sized tumor. The results show that the tumor can be detected with high accuracy by relying on the coordinates of the maximum value of SAR. The maximum SAR is also analyzed at distinct tumor locations at various frequency ranges. Thus the breast cancer detection system employing the shaped pulse using the proposed pulse shaper is potentially useful in identifying the location of tumor, especially when they are of smaller size of 1mm radius. Analysis on the variations in maximum SAR and electric field intensity for various frequencies of UWB pulse inside homogeneous fibroglandular layer of breast phantom

showed that lower frequencies provide greater penetration depth but lesser location accuracy of tumor and vice versa. Experimental validation using fabricated breast phantom with monostatic radar shows good variation in S11 parameters with and with out tumor in the frequency band 3.6-5.4 GHz indicating presence of tumor. This closely matches with simulation results. Future work will focus on experimental verification of the technique on various breast phantoms based on patient variability as a step towards clinical trials. More approaches to achieve better discrimination between benign and malignant tumors can be considered.

ACKNOWLEDGMENT

The authors would like to thank the Centre of Excellence in E-Mobility, School of Engineering and Technology, CHRIST (Deemed to be University), Kengeri, Bengaluru, India.

REFERENCES

[1] R. Chávez-Santiago, I. Balasingham, and J. Bergsland, "Ultrawideband technology in medicine: A survey," *J. Electr. Comput. Eng.*, vol. 2012, Apr. 2012, Art. no. 716973.

[2] E. M. Staderini, "UWB radars in medicine," *IEEE Aerosp. Electron. Syst. Mag.*, vol. 17, no. 1, pp. 13–18, Jan. 2002.

[3] X. Yong, L. Yinghua, Z. Hongxin, and W. Yeqiu, "An overview of ultra-wideband technique application for medial engineering," in *Proc. IEEE/ICME Int. Conf. Complex Med. Eng.*, May 2007, pp. 408–411.

[4] S. M. Chouiti, L. Merad, S. M. Meriah, X. Raimundo, and A. Taleb-Ahmed, "An efficient image reconstruction method for breast cancer detection using an ultra-wideband microwave imaging system," *Electromagnetics*, vol. 36, no. 4, pp. 225–235, May 2016, doi: 10.1080/02726343.2016.1158612.

[5] A. Khaleghi, R. Chávez-Santiago, and I. Balasingham, "Ultra-wideband pulse-based data communications for medical implants," *IET Commun.*, vol. 4, no. 15, pp. 1889–1897, Oct. 2010.

[6] T.-A. Phan, V. Krizhanovskii, S.-K. Han, S.-G. Lee, H.-S. Oh, and N.-S. Kim, "4.7pJ/pulse 7^{th} derivative Gaussian pulse generator for impulse radio UWB," in *Proc. IEEE Int. Symp. Circuits Syst.*, May 2007, pp. 3043–3046.

[7] H. Sheng, P. Orlik, A. M. Haimovich, L. J. Cimini, and J. Zhang, "On the spectral and power requirements for ultra-wideband transmission," in *Proc. IEEE Int. Conf. Commun. (ICC)*, May 2003, pp. 738–742.

[8] M. Rezaii, "UWB pulse shaping by FIR filter to enhance power efficiency," in *Proc. IEEE 5th Int. Symp. Wireless Pervasive Comput.*, May 2010, pp. 522–527.

[9] B. Hu and N. C. Beaulieu, "Pulse shapes for ultrawideband communication systems," *IEEE Trans. Wireless Commun.*, vol. 4, no. 4, pp. 1789–1797, Jul. 2005.

[10] M. Cavagnaro, E. Pittella, and S. Pisa, "UWB pulse propagation into human tissues," *Phys. Med. Biol.*, vol. 58, no. 24, p. 8689, Nov. 2013.

[11] I. E. Khuda, "Modeling and simulation of UWB wave propagation for early detection of breast tumors in cancer dielectric imaging systems," *Eng. J.*, vol. 21, no. 2, pp. 237–251, Mar. 2017.

[12] M. K. D. Menon, J. Rodrigues, and L. J. Gudino, "Synthesis of UWB pulse shaper for efficient pulse propagation in human tissue," in *Proc. 12th Int. Symp. Commun. Syst., Netw. Digit. Signal Process. (CSNDSP)*, Jul. 2020, pp. 1–5.

[13] Y. Lim, "Frequency-response masking approach for the synthesis of sharp linear phase digital filters," *IEEE Trans. Circuits Syst.*, vol. CS-33, no. 4, pp. 357–364, Apr. 1986.

[14] J. Rodrigues and K. R. Pai, "New approach to the synthesis of sharp transition fir digital filter," in *Proc. IEEE Int. Symp. Ind. Electron.*, Jun. 2005, pp. 1171–1173.

[15] J. X. Rodrigues and K. R. Pai, "Modified linear phase frequency response masking FIR filter," in *Proc. 4th Int. Symp. Image Signal Process. Anal. (ISPA)*, 2005, pp. 434–439.

[16] X. Liu, A. B. Premkumar, and A. S. Madhukumar, "Pulse shaping functions for UWB systems," *IEEE Trans. Wireless Commun.*, vol. 7, no. 5, pp. 1512–1516, May 2008.

[17] R. S. A. R. Abdullah, O. N. Samijayani, S. Adabi, A. Ismail, M. I. Saripan, and S. A. Alshehri, "Breast tumor detection using microwave ultra wideband (UWB) forward scattering radar system," *Int. J. Phys. Sci.*, vol. 7, no. 64, pp. 6062–6074, Dec. 2012. [Online]. Available: https://academicjournals.org/journal/IJPS/article-abstract/4D242C418927

[18] S. Fouad, R. Ghoname, A. E. Elmahdy, and A. E. Zekry, "Enhancing tumor detection in IR-UWB breast cancer system," *Int. Scholarly Res. Notices*, vol. 2017, Mar. 2017, Art. no. 4606580.

[19] G. Varotto and E. M. Staderini, "On the UWB medical radars working principles," *Int. J. Ultra Wideband Commun. Syst.*, vol. 2, no. 2, pp. 83–93, Jan. 2011.

[20] M. A. Aldhaeebi, K. Alzoubi, T. S. Almoneef, S. M. Bamatraf, H. Attia, and O. M. Ramahi, "Review of microwaves techniques for breast cancer detection," *Sensors*, vol. 20, no. 8, p. 2390, Apr. 2020. [Online]. Available: https://www.mdpi.com/1424-8220/20/8/2390

[21] U. Rafique, S. Pisa, R. Cicchetti, O. Testa, and M. Cavagnaro, "Ultra-wideband antennas for biomedical imaging applications: A survey," *Sensors*, vol. 22, no. 9, p. 3230, Apr. 2022.

[22] G. K. Pandey, H. S. Singh, P. K. Bharti, A. Pandey, and M. K. Meshram, "High gain Vivaldi antenna for radar and microwave imaging applications," *Int. J. Signal Process. Syst.*, vol. 3, no. 1, pp. 35–39, 2014.

[23] J. Bourqui, M. Okoniewski, and E. C. Fear, "Balanced antipodal Vivaldi antenna for breast cancer detection," in *IET Seminar Dig.*, 2007, pp. 1–5.

[24] M. Kanjaa, O. El Mrabet, M. Khalladi, and M. Essaaidi, "Exponentially tapered antipodal Vivaldi antenna for breast cancer detection," in *Proc. IEEE 15th Medit. Microw. Symp. (MMS)*, Nov. 2015, pp. 1–3.

[25] J. Bourqui, M. Okoniewski, and E. C. Fear, "Balanced antipodal Vivaldi antenna with dielectric director for near-field microwave imaging," *IEEE Trans. Antennas Propag.*, vol. 58, no. 7, pp. 2318–2326, Jul. 2010.

[26] J. Bourqui, M. A. Campbell, T. Williams, and E. C. Fear, "Antenna evaluation for ultra-wideband microwave imaging," *Int. J. Antennas Propag.*, vol. 2010, May 2010, Art. no. 850149.

[27] B. Biswas, R. Ghatak, and D. R. Poddar, "A fern fractal leaf inspired wideband antipodal Vivaldi antenna for microwave imaging system," *IEEE Trans. Antennas Propag.*, vol. 65, no. 11, pp. 6126–6129, Nov. 2017.

[28] M. T. Islam, M. Z. Mahmud, N. Misran, J.-I. Takada, and M. Cho, "Microwave breast phantom measurement system with compact side slotted directional antenna," *IEEE Access*, vol. 5, pp. 5321–5330, 2017.

[29] A. M. D. Oliveira, J. F. Justo, M. B. Perotoni, S. T. Kofuji, A. G. Neto, R. C. Bueno, and H. Baudrand, "A high directive Koch fractal Vivaldi antenna design for medical near-field microwave imaging applications," *Microw. Opt. Technol. Lett.*, vol. 59, no. 2, pp. 337–346, Feb. 2017.

[30] B. V. Kadam, L. J. Gudino, C. K. Ramesha, and J. X. Rodrigues, "Single port multimode reconfigurable UWB-NB antenna for cognitive radio applications," *J. Microw., Optoelectron. Electromagn. Appl.*, vol. 21, no. 4, pp. 623–638, Dec. 2022.

[31] M. Lazebnik, D. Popovic, L. McCartney, C. B. Watkins, M. J. Lindstrom, J. Harter, S. Sewall, T. Ogilvie, A. Magliocco, T. M. Breslin, W. Temple, D. Mew, J. H. Booske, M. Okoniewski, and S. C. Hagness, "A large-scale study of the ultrawideband microwave dielectric properties of normal, benign and malignant breast tissues obtained from cancer surgeries," *Phys. Med. Biol.*, vol. 52, no. 20, pp. 6093–6115, Oct. 2007.

[32] M. Lazebnik, M. Okoniewski, J. H. Booske, and S. C. Hagness, "Highly accurate Debye models for normal and malignant breast tissue dielectric properties at microwave frequencies," *IEEE Microw. Wireless Compon. Lett.*, vol. 17, no. 12, pp. 822–824, Dec. 2007.

[33] J. A. Basurto-Hurtado, I. A. Cruz-Albarran, M. Toledano-Ayala, M. A. Ibarra-Manzano, L. A. Morales-Hernandez, and C. A. Perez-Ramirez, "Diagnostic strategies for breast cancer detection: From image generation to classification strategies using artificial intelligence algorithms," *Cancers*, vol. 14, no. 14, p. 3442, Jul. 2022.

[34] *UWCEM—Phantom Repository*. Accessed: Jun. 5, 2023. [Online]. Available: https://uwcem.ece.wisc.edu/phantomRepository.html

[35] A. Martellosio, M. Pasian, M. Bozzi, L. Perregrini, A. Mazzanti, F. Svelto, P. E. Summers, G. Renne, L. Preda, and M. Bellomi, "Dielectric properties characterization from 0.5 to 50 GHz of breast cancer tissues," *IEEE Trans. Microw. Theory Techn.*, vol. 65, no. 3, pp. 998–1011, Mar. 2017.

[36] S. Gabriel, R. W. Lau, and C. Gabriel, "The dielectric properties of biological tissues: III. Parametric models for the dielectric spectrum of tissues," *Phys. Med. Biol.*, vol. 41, no. 11, pp. 2271–2293, Nov. 1996.

[37] K. Sasaki, K. Wake, and S. Watanabe, "Development of best fit Cole-Cole parameters for measurement data from biological tissues and organs between 1 MHz and 20 GHz," *Radio Sci.*, vol. 49, no. 7, pp. 459–472, Jul. 2014.
[38] I. Amdaouch, M. Saban, J. El Gueri, M. Z. Chaari, A. V. Alejos, J. R. Alzola, A. R. Muñoz, and O. Aghzout, "A novel approach of a low-cost UWB microwave imaging system with high resolution based on SAR and a new fast reconstruction algorithm for early-stage breast cancer detection," *J. Imag.*, vol. 8, no. 10, p. 264, Sep. 2022.
[39] D. Bhargava and P. Rattanadecho, "Microwave imaging of breast cancer: Simulation analysis of SAR and temperature in tumors for different age and type," *Case Stud. Thermal Eng.*, vol. 31, Mar. 2022, Art. no. 101843.
[40] R. Krishnan and J. Christ, "An investigation using specific absorption rate analysis to diagnose early-stage breast tumor using UWB antenna," *Current Med. Imag. Formerly Current Med. Imag. Rev.*, vol. 17, no. 12, pp. 1425–1431, Dec. 2021.
[41] H. Peng, C. Wang, L. Zhao, and J. Liu, "Novel SRR-loaded CPW-fed UWB antenna with wide band-notched characteristics," *Int. J. Microw. Wireless Technol.*, vol. 9, no. 4, pp. 875–880, May 2017.
[42] M. Aminudin Jamlos, W. A. Mustafa, W. Khairunizam, I. Zunaidi, Z. M. Razlan, and A. B. Shahriman, "Tumor detection via specific absorption rate technique using ultra-wideband antenna," *IOP Conf., Mater. Sci. Eng.*, vol. 557, Jun. 2019, Art. no. 012024.
[43] L. M. Surhone, M. T. Tennoe, and S. F. Henssonow, *Specific Absorption Rate*. Beau-Bassin: Betascript Publishing, Jun. 2011.
[44] N. T. H. Trang, K. Q. Long, P. L. An, and T. N. Dang, "Development of an artificial intelligence-based breast cancer detection model by combining mammograms and medical health records," *Diagnostics*, vol. 13, no. 3, p. 346, Jan. 2023.
[45] D. U. Ozsahin, D. I. Emegano, B. Uzun, and I. Ozsahin, "The systematic review of artificial intelligence applications in breast cancer diagnosis," *Diagnostics*, vol. 13, no. 1, p. 45, Dec. 2022.
[46] C. Chakraborty, A. Kishor, and J. J. P. C. Rodrigues, "Novel Enhanced-Grey Wolf Optimization hybrid machine learning technique for biomedical data computation," *Comput. Electr. Eng.*, vol. 99, Apr. 2022, Art. no. 107778.
[47] C. Chakraborty, B. Gupta, and S. K. Ghosh, "Chronic wound characterization using Bayesian classifier under telemedicine framework," *Int. J. E-Health Med. Commun.*, vol. 7, no. 1, pp. 76–93, Jan. 2016.
[48] M. T. Islam, M. Samsuzzaman, S. Kibria, and M. T. Islam, "Experimental breast phantoms for estimation of breast tumor using microwave imaging systems," *IEEE Access*, vol. 6, pp. 78587–78597, 2018.
[49] P. Agoramurthy and R. Sundararajan, "Electric field distribution of human breast tissue," in *Proc. Annu. Rep. Conf. Electr. Insul. Dielectric Phenomena*, Oct. 2010, pp. 1–4.
[50] V. G. Sree, K. Udayakumar, and R. Sundararajan, "Electric field analysis of breast tumor cells," *Int. J. Breast Cancer*, vol. 2011, Dec. 2011, Art. no. 235926.
[51] A. Sharma and S. K. Sharma, "Spectral efficient pulse shape design for UWB communication with reduced ringing effect and performance evaluation for IEEE 802.15.4a channel," *Wireless Netw.*, vol. 25, no. 5, pp. 2723–2740, Jul. 2019.
[52] M. K. D. Menon and J. Rodrigues, "Pulse shaper design for UWB-based medical imaging applications," *Communication and Intelligent Systems* (Lecture Notes in Networks and Systems), vol. 461. India: Springer, 2022, pp. 897–907.
[53] R. Chavez-Santiago, A. Khaleghi, I. Balasingham, and T. A. Ramstad, "Architecture of an ultra wideband wireless body area network for medical applications," in *Proc. 2nd Int. Symp. Appl. Sci. Biomed. Commun. Technol.*, Nov. 2009.
[54] F. Alsharif and C. Kurnaz, "Wearable microstrip patch ultra wide band antenna for breast cancer detection," in *Proc. 41st Int. Conf. Telecommun. Signal Process. (TSP)*, Jul. 2018, pp. 1–5.

M. K. DEVIKA MENON received the B.Tech. degree in electrical and electronics engineering from the University of Kerala, India, in 2009, and the M.Tech. degree in power electronics from Amritha Vishwa Vidya Peetham University, Coimbatore, India, in 2011. She is currently pursuing the Ph.D. degree in electrical engineering with CHRIST(Deemed to be University), Bengaluru, India. Since 2012, she has been an Assistant Professor with the Department of Electrical and Electronics Engineering, CHRIST (Deemed to be University). Her research interests include the application of digital signal processing in biomedical engineering, control systems, and power electronics. She has presented research papers in several international conferences and has done publications in peer reviewed journals and book chapters. She has received research grant award for 12th IEEE/IET International Symposium on Communication Systems, Networks and Digital Signal Processing-CSNDSP 2020, Porto, Portugal.

JOSEPH RODRIGUES received the B.E. degree in electrical engineering from the BVB College of Engineering, Hubli, India, the M.Tech. degree in power electronics from the National Institute of Technology, Calicut, and the Ph.D. degree from Goa University, India, in 2006. Since 2016, he has been a Professor and the Head of the Department of Electrical and Electronics Engineering, School of Engineering and Technology, CHRIST (Deemed to be University), Bengaluru, India. He has more than 25 publications in reputed peer reviewed journals, around 35 reputed international conference publications and book chapters. He has won best paper awards and travel grants to present papers at international conferences and has travelled extensively. He has guided several U.G., P.G. dissertations, and guiding Ph.D. scholars. His research interests include digital filter design, signal processing applications in biomedical and wireless communications, wireless sensor networks, and vehicular sensor networks.